People Tracking in Ambient Assisted Living Environments Using Low-Cost Thermal Image Cameras

Christian Mandel(✉) and Serge Autexier

German Research Center for Artificial Intelligence,
Cyber Physical Systems Cartesium {0.51/1.49}, Enrique-Schmidt-Str. 5,
28359 Bremen, Germany
{Christian.Mandel,Serge.Autexier}@dfki.de

Abstract. In this paper we propose the use of low-cost thermal imaging sensors for the application of people tracking in Ambient Assisted Living environments. We describe background subtraction and segmentation on low-resolution thermal images as the necessary preprocessing steps to derive suitable percepts. Extensive data association to samples of a set of Monte-Carlo particle filters is realized by circle-circle intersection tests between percepts and pose hypotheses. Experimental evaluation conducted in the Bremen Ambient Assisted Living Lab proves the precision of the proposed system by comparing the tracking results against ground truth data coming from an ARTTRACK optical tracking system.

Keywords: Tracking system · Thermal camera · Data association · Particle filter · Ambient assisted living

1 Introduction

Age-appropriate assistance systems for self-determined living is a key focus of the *Bremen Ambient Assisted Living Lab* (BAALL) [2]. People with mobility impairments are supported by providing intelligent mobility devices that are embedded in the apartment [10]. Appliances such as lights, doors, height-adjustable cabinets, and mirrors are becoming intelligent through mutual interconnection and control. All of these applications depend on, or benefit from, the knowledge about the spatial location of their users. For instance, a wheelchair can be sent to a goal to pickup a person if the person's initial location is known, and ceiling lights can be controlled such that only the direct surrounding of a person's location is lit at a time.

While the aforementioned mobility devices, i.e. wheelchairs and walkers, localize themselves and their users by matching readings from on board laser range finders against map data (cf. the *GMapping* approach in [8]), pure people localization should be realized without instrumenting the persons to be tracked.

C.K. Chang et al. (Eds.): ICOST 2016, LNCS 9677, pp. 14–26, 2016.
DOI: 10.1007/978-3-319-39601-9_2

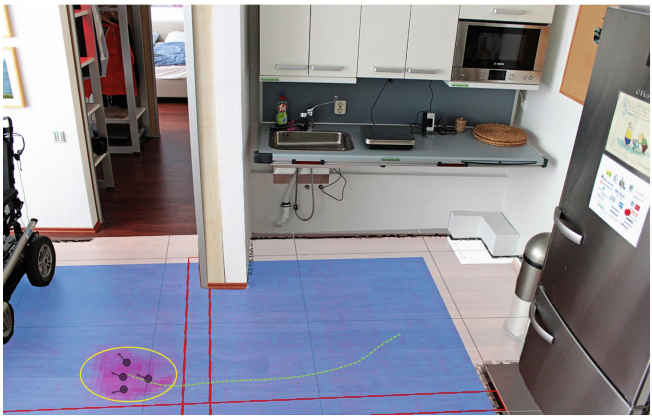

Fig. 1. Illustration of essential methods used in this work: a thermal camera mounted at the ceiling of the depicted kitchen area perceives the superimposed video image. The blue area contrasts to the thermal signature of a person rendered by a red pixel cluster. This cluster is abstracted by the yellow circular-shaped percept, and fed into a Monte-Carlo particle filter that tracks the green colored trajectory of the Subject. (Color figure online)

Initial experiments in this direction solely required the user to carry a smartphone that received signals from *Bluetooth Low Energy*-beacons mounted in the BAALL, in order to realize fingerprinting-based localization (cf. [13]).

Therefore, this paper proposes the use of downward facing thermal cameras mounted at the ceiling of the apartment. We will show that the stream of low-resolution (80×60 pixels) thermal images can be utilized to successfully track people in the BAALL by feeding them into a set of multi-hypotheses *Monte-Carlo* particle filters (cf. Fig. 1 for the application scenario). Please note that tracking does not imply to recognize individual persons from a trained set.

The remainder of this article is structured as follows: Sect. 2 gives an overview on state of the art approaches in visual people tracking, including thermal camera-based solutions. Section 3 overviews our solution of a Monte-Carlo particle filter-based tracking system that works on thermal camera percepts. Section 4 details the methods proposed by our work, namely thermal camera image preprocessing, data association between image percepts and particle filter hypotheses, and the actual tracking algorithm. In Sect. 5 we describe the experimental evaluation, including a comparison of tracking results between our proposed method and the gold standard, an *ARTTRACK* optical tracking solution. The latter tracks retroreflective markers fixed on the subjects. We finally conclude with Sect. 6 by discussing the achieved results and future work.

2 Related Work

A good starting point for dealing with people localization services in Ambient Assisted Linving environments is given by Eisa and Moreira. In [4] they define requirements and metrics for AAL related localization techniques.

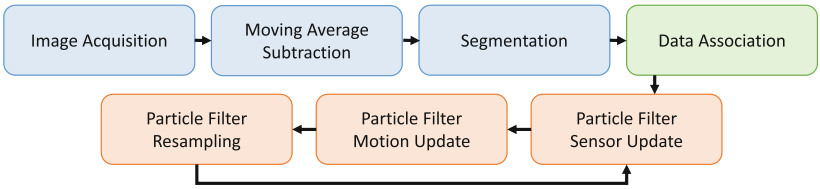

Fig. 2. Flowchart diagram of the people tracking system described in this paper. The software is structured into image acquisition and preprocessing steps (blue), data association (green), and the particle filter cycle (red). (Color figure online)

In [9], Hevesi et al. describe a system that makes use of cheap arrays of infrared sensors (8×8 pixels) for people localization with an accuracy of 1 m in home and office environments. By classifying time series of temperature feature vectors, it is also possible to monitor household appliances such as water cookers. Tracking of multiple sources of heat while recognizing their identity is not described.

Kumar et al. [11] also use a low resolution thermal sensor consisting of 32 single infrared receivers for people tracking in indoor environments. By rotating the linear system about 140° in 94 discrete steps, they construct a 2-dimensional image in one minute. After fusing blobs from the infrared image with a 640×480 pixel wide RGB image, the results of pure RGB-based template tracking can be improved. Since track identity is not handled by the system, this work is more about estimating the location of people in image frames.

A performance comparison between Kalman filter and particle filter-based optical people tracking approaches is given by Bazzani et al. in [3]. Although working on RGB-image datasets and not on monochromatic thermal images, and thus dealing with different strategies for background subtraction and percept modeling, this work motivates the application of the particle filter method since it shows a better *tracking success rate*.

Beside the research perspective, people localization and tracking in ambient assisted living environments is already a commercial issue. Therefore, actual research and developments have to prevail against already available solutions, e.g. the people tracking flooring material *SensFloor* [7].

The contribution of our own work is straightforward. We describe a particle-filter-based tracking system with an accuracy that is well-suited for security and convenience appliances in ambient assisted living environments. In spite of the low resolution sensorial input, we can prove a mean error of < 12 cm compared to a sophisticated marker-based optical tracking system that served

as our ground truth. From this perspective, we can enhance the performance of available thermal sensor-based tracking solutions.

3 System Overview

The thermal imaging sensor setup as shown in Fig. 3 is mounted in a height of 4.4 m under the ceiling of the BAALL, but over a suspended ceiling made of textile that is opaque for the human eye, but transparent for the infrared spectrum of electromagnetic radiation. Hardly noticeable for visitors of the flat, the thermal camera observes approximately $6m^2$ of the kitchen area. According to Fig. 2, image acquisition is the first step of our proposed tracking system (see Sect. 4.1). Running as a C++ application on a Raspberry Pi, this step reads out the thermal images from the sensor, and forwards the video stream to a PC running the next steps under the robotics framework *SimRobot* [12].

Thermal images are now preprocessed by first increasing contrast through static background subtraction (cf. Sect. 4.2). The following segmentation process outputs blobs that are candidates for people silhouettes. Abstracted by encompassing circles, these percepts are associated to hypotheses of particle filters that each track a single person. The data association described in Sect. 4.3 builds on the assumption that a given percept better explains a sample if the area of intersection between the two circles is large. Since even multiple percepts can explain a single hypothesis about the position of a person, the particle filter's sensor update step (cf. Sect. 4.4) computes the sample's weight by summing up the total area of intersection with all percepts associated to this sample.

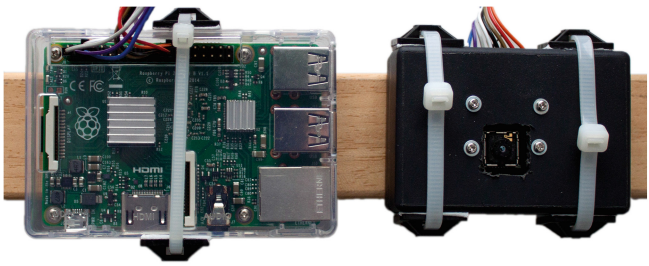

Fig. 3. The experimental sensor setup includes a boxed *FLiR Lepton* longwave imaging module (right), and a connected *Raspberry Pi 2 Model B* (left) for initial data acquisition. The Pi is also used for forwarding the video stream to a computer running the preprocessing and tracking algorithms.

4 Detailed System Description

4.1 Sensorial Equipment

For acquiring thermal images, we use a *FLiR Lepton* longwave infrared imaging module that connects via a breakout board to a *Raspberry Pi 2 Model B*.

The Lepton (cf. [5] for a more detailed description) is based on a microbolometer focal plane array, and is capable of outputting 80×60 pixels with a thermal sensitivity of $< 50\,\text{mK}$. Given the sensor's $51°$ wide horizontal, and $63.5°$ wide diagonal field of view, our application scenario asks for a sufficiently high mounting position in order to cover a preferably large area on the ground plane of the room observed. Please note that the camera doesn't output absolute temperature values per pixel. Instead, the sensor maps the observed temperature spectrum to a 14 bit wide range, and sets each pixel to a value within this interval. After basic image data collection is performed by the Raspberry Pi, the video stream is transfered to a PC via a TCP/IP stream. We have selected this multi-host solution for the reason of convenience, i.e. the Raspberry Pi and the camera module can stay online mounted on the ceiling, while code changes in the preprocessing and filtering part is done on a development PC.

4.2 Preprocessing of Raw Images

A typical raw image coming from the thermal camera can be seen in Fig. 4 (left). Beside the desired information, raw images contain undesirable properties that are tackled during the preprocessing steps.

The first major drawback of raw images is given by picture fragments that depict sources of heat different from the human body, e.g. the upper left pixel blob in Fig. 4 (left) that is caused by the motor of a fridge. Although we cannot decide the question which one of the two image fragments equal in shape and temperature is originating from a person's silhouette, and which one not, it is possible to filter out image portions that present a static temperature over time.

A further artifact that complicates the recognition of thermal signatures caused by persons is given by a global temperature gradient caused by the camera or the sun's thermal radiation passing through windows into the scene. An exemplary situation is shown in Fig. 4 (left), where the gradient extends from the upper right corner to the lower left corner.

Both artifacts described are tackled by background subtraction. The resulting images (see Fig. 4 (centre) for an example) show an increased contrast between foreground objects and background, and are taken as the input for the segmentation process. After segmentation, images are represented by blobs, i.e. pixel-groups sharing the same flattened temperature value (cf. Fig. 4 (right)).

Background Subtraction. By subtracting the moving average temperature of a given pixel, from the current temperature reading of the same pixel, we obtain values that tend towards 0 for static background pixel, and values $\neq 0$ for foreground pixels. The moving average filter is implemented as in (1), and (2). Here, $ma^t_{x,y}$ denotes the moving average of the pixel located at position (x, y), at time t. The current reading at the same location is given by $p^t_{x,y}$ and $bsp^t_{x,y}$ is the value after background subtraction. The parameter $c \in [0..1]$ describes how strong the actual reading influences the moving average.

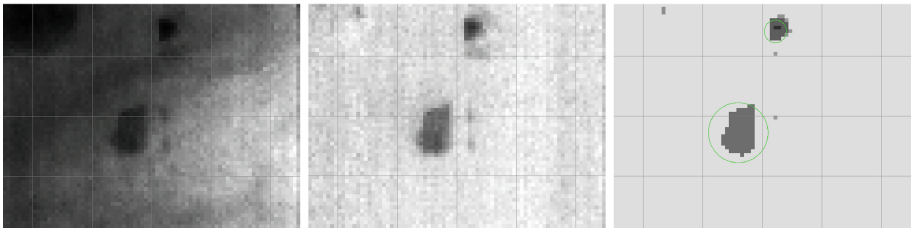

Fig. 4. Illustration of thermal image preprocessing pipeline - *Left*: Raw image as outputted from the sensor. Warm areas render dark, while colder areas render light. This image depicts two persons, one in the center and one to the upper right. The dark area to the upper left originates from a static source of heat. *Centre*: After background subtraction, the static source of heat, as well as an image wide thermal gradient, caused by sensor miss-calibration, disappears. *Right*: Segmentation yields two blobs describing the persons observed by center coordinates and a maximal radius.

$$ma^t_{x,y} = c\, p^t_{x,y} + (1-c)\, ma^{t-1}_{x,y} \tag{1}$$

$$bsp^t_{x,y} = \left| p^t_{x,y} - ma^t_{x,y} \right| \tag{2}$$

Segmentation. This step is implemented by recursively processing each pixel via an 8-neighbor connectedness. A neighboring pixel is assigned to the center pixel's blob, if it has not been visited so far, and if its temperature value differs from the blob's mean temperature no more than a given threshold. After including a new pixel into an existing blob, the temperature values of all of the blob's pixels are set to the blob's mean temperature. If an unvisited pixel is not recorded into the currently processed blob, a new blob is opened by that pixel.

4.3 Data Association

The key task of data association is to assign percepts generated from preprocessed images to pose hypotheses of the tracking filters (cf. Sect. 4.4) for validation. Basically a percept is given by a pixel blob that might correspond to a person's silhouette, i.e. it matches in size and mean temperature the expected values. We abstract a percept by the smallest circle that contains all blob pixels. Thus, we define the structure of a percept as follows:

$$\mathcal{P}_t = [(x_t, y_t), r_t, t_t, \mathcal{S}_t] \tag{3}$$

In (3), $\mathcal{S}_t$ denotes the set of blob-pixels the percept is generated from, (x_t, y_t) and r_t the center and radius of a circle that encompasses $\mathcal{S}_t$, and t_t the mean temperature of $\mathcal{S}_t$. Our basic strategy for judging whether or not a given percept supports a pose hypothesis of a tracked person, that is modeled by a circle as well, is to calculate the overlapping area between the circles involved. According to that, let d be the distance between the midpoints of two circles with radii

r_1 and r_2. Then, according to [14], the area of intersection A between the two circles is given as in (4).

$$A = r_1^2 \cos^{-1}\left(\frac{d^2 + r_1^2 - r_2^2}{2dr_1}\right) + r_2^2 \cos^{-1}\left(\frac{d^2 + r_2^2 - r_1^2}{2dr_2}\right) - \frac{1}{2}\sqrt{(-d + r_1 + r_2)(d + r_1 - r_2)(d - r_1 + r_2)(d + r_1 + r_2)} \quad (4)$$

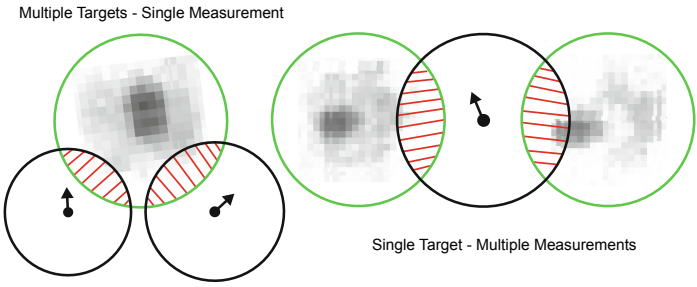

Fig. 5. Illustration of two cases where image segmentation fails to produce suitable percepts for the given situation. The red area describes the intersection between the percepts modeled by green circles, and the pose hypotheses modeled by black circles. (Color figure online)

Beside the trivial case in which one percept overlaps with exactly one hypothesis of an already existing filter, data association handles the following situations:

1. Multiple Targets - Single Measurement: This case (cf. Fig. 5 (left)) typically occurs in situations where two persons that are already tracked by their individual filter move close together. Image segmentation produces a single blob that describes the merged shape of both individuals.
2. Single Target - Multiple Measurements: In this situation (cf. Fig. 5 (right)) image segmentation has failed to produce a single blob for the silhouette of a person. Instead, two separate blobs explain a pose hypothesis.
3. No Match: Since there is no filter with at least one hypothesis that explains the given percept $\mathcal{P}_t$, a new filter is instantiated. The samples of the new particle filter are initialized at (x_t, y_t) of the given percept $\mathcal{P}_t$.

Occlusion Handling. A special case for *single target - multiple measurements* data association is given by partly occluded silhouettes. Because of the suspended ceiling's beams in-between the camera and the persons to be tracked (cf. Fig. 7 (right)), pixel blobs describing a single target are split sometimes (cf. Fig. 6 for an illustration). Since the general rule of data association requires an overlap between the percept's and the sample's circles, which is obviously not given in this situation, a different strategy is necessary. Therefore, we model the

static beams of the suspended ceiling by rectangles in world space. After also transforming the image percepts into world space, we check for the number of intersections between a line that connects a sample's position with a percept's position, and the beam rectangle's lines. If we can conclude that both circles are located on different sides of the beam, and if they are no more separated than a given threshold, the percept is attached to the sample and adds to its weighting.

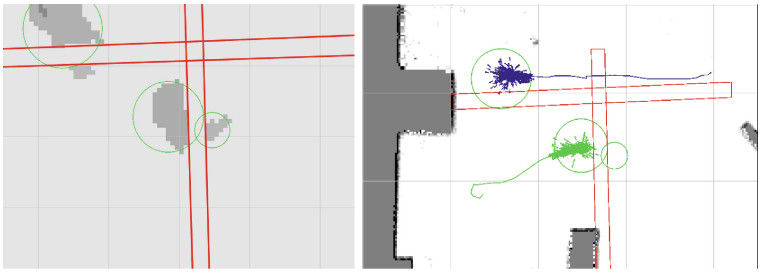

Fig. 6. Illustration of percepts that are partly occluded by beams of the suspended ceiling in-between the camera and the person to be tracked. Red colored rectangles model the beams that can also be seen in Fig. 7(right). (Color figure online)

4.4 Monte-Carlo Particle Filter Tracking

We chose the Monte-Carlo particle filter approach [6] to track people's trajectories, since this algorithm is able to deal with the non-linear motion model involved, and its ability to handle multiple hypotheses. Let a single hypothesis about the position and orientation of a tracked person at point of time t be described by the sample $s_t = [(x_t, y_t), \theta_t, r_t, \omega_t]$. The vector (x_t, y_t) denotes the cartesian position in the ground-parallel plane, and θ_t the direction of movement, which we interprete as the person's orientation w.r.t. the global x-coordinate axis. Furthermore, r_t represents the mean radius of all circular percepts that confirmed s_t, and ω_t the weighting, or probability that s_t describes a person respectively. A single particle filter is now defined as $PF_t = [S_t, P_t]$, with $S_t = \{s_t^1, ..., s_t^m\}$ describing the discrete probability distribution about the position and orientation of a tracked person by m samples, and $P_t = \{p_{t-n}, ..., p_t\}$ describing the path of this filter, i.e. the list of the mean positions over all samples during the last n cycles of *sensor update*, *motion update*, and *resampling*. Above, the parameter n is chosen freely for informational purposes only.

Sensor Update. Since data association has already assigned the set of percepts $\{\mathcal{P}_t^1, \ldots, \mathcal{P}_t^i\}$ that overlap with the sample under scope, computing the sample's weight ω_t^m is straightforward given the following formula:

$$\omega_t^m = \mathcal{N}\left(0, \sigma^2\right)\left(1 - \min\left(1, \frac{\sum_{i=1}^{n} A\left(s_t^m\right) \cap A\left(\mathcal{P}_t^i\right)}{A\left(s_t^m\right)}\right)\right) \tag{5}$$

In (5), the inner fraction describes the relative area of the sample's circle that is covered by all of the percepts attached. By adjusting σ, one can let even small overlaps produce a good weighting, or favor only extensive overlaps respectively.

Motion Update. A sample's state transition through motion is given by

$$u_t^m \models \langle d_t, h_t \rangle \tag{6}$$

with d_t being the translational distance walked since the last motion update, and h_t being the rotational distance respectively. Note that we do not use a real odometry sensor, e.g. a gait detector, at this point. Instead, we assume the traveled distance to be given by the distance from the mean center of all percepts associated to sample m at time t, to the location of sample m at time $t-1$. A 3-dimensional movement vector $v^m = (v_x^m, v_y^m, v_\theta^m)$ is now computed as follows:

$$v^m = \begin{pmatrix} M_\theta^m \begin{pmatrix} d_t + a_1 n_x^m(d_t) \\ a_2 n_y^m(d_t) \end{pmatrix} \\ a_3 n_\theta^m(h_t) \end{pmatrix} \tag{7}$$

In (7), M_θ^m denotes a rotation matrix that describes the sample's orientation θ^m, $n_{x,y,\theta}^m$ noise functions sampled from a triangular distribution, and a_1, a_2, a_3 three different scalars for the generated noise.

$$x_t^m = x_{t-1}^m + v_x^m \tag{8}$$

$$y_t^m = y_{t-1}^m + v_y^m \tag{9}$$

$$\theta_t^m = \theta_{t-1}^m + v_\theta^m \tag{10}$$

With the movement vector v^m described in (7), a sample's new position and orientation is computed according to (8), (9), and (10).

Resampling. Samples from each particle filter are carried over to the next cycle of computation according to their weighting. This means, that hypotheses with a high weighting are cloned, while hypotheses with a low weighting disappear.

5 Experimental Evaluation

In order to prove the accuracy of the tracking system proposed in this work, we compared its results from an experimental evaluation with the output of an *A.R.T. DTrack2* reference tracking system [1]. The DTrack2 tracking system configuration consisted of two cameras actively sending out infrared light at 880 nm wavelength, which is well reflected by retro reflective markers. The spherical markers that were used had a diameter of 30 mm, and were fixed on top of a cap worn by the tracked person. After calibration of the DTrack2 system, three-dimensional marker positions were outputted at 60 Hz.

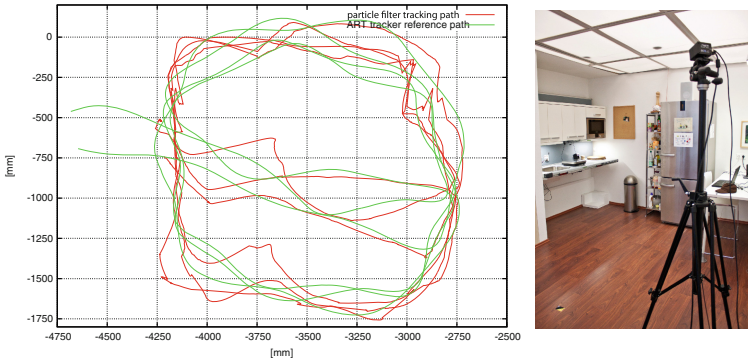

Fig. 7. Comparison of paths tracked by the thermal image percepts driven particle filter, and a DTrack2 optical tracking system (left). The evaluation took place in the kitchen area of the BAALL (right). Here, one person walked clockwise and counter-clockwise rounds between the table and the kitchen bench.

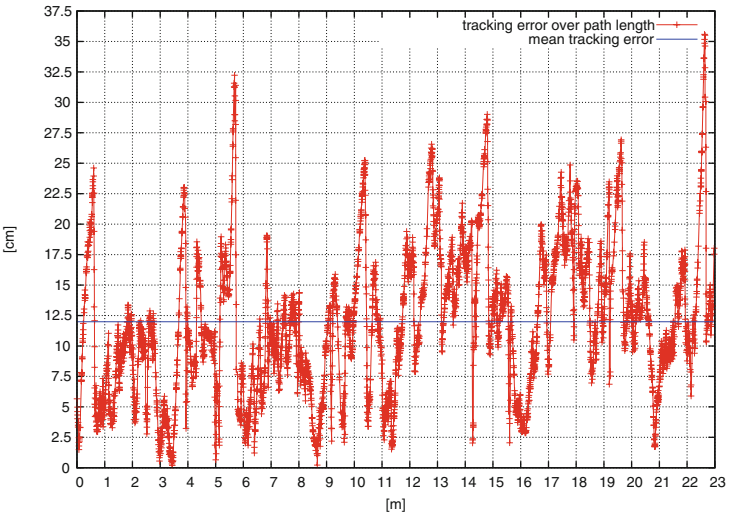

Fig. 8. Error plot indicating the performance of the tracking system proposed in this work. The red curve depicts the distance between associated points along the paths outputted by the A.R.T. DTrack2 system, and our approach (cf. Fig. 7(left)). Given the DTrack2 ground truth, we observed a minimal, maximal, and mean error of $\varepsilon_{\min} \approx 1.94\,\text{mm}$, $\varepsilon_{\max} \approx 35.58\,\text{cm}$, and $\bar{\varepsilon} \approx 11.91\,\text{cm}$, along the $d \approx 23\,\text{m}$ long path. (Color figure online)

Starting at the kitchen table, the test person walked approximately 23 m in two clock-wise and two counter-clockwise oriented circles located in-between the table and the kitchen bench (cf. Fig. 7 (right)). During that walk, the probandee was observed by the DTRack2 system described above, and the thermal

image-based tracking system proposed in this work. In order to allow for comparison of the results, tracking output of both systems was transformed into a common two-dimensional coordinate system (cf. Fig. 7 (left)).

We observed a mean deviation of $\bar{\varepsilon} \approx 11.91\,\text{cm}$ between our particle filter-based tracking and the DTRack2 ground truth (cf. Fig. 8). The maximal error observed was $\varepsilon_{\max} \approx 35.58\,\text{cm}$, while the minimal error is given by $\varepsilon_{\min} \approx 1.94\,\text{mm}$.

Multi people tracking has only been roughly examined so far, with a maximum of three subjects simultaneously moving in the viewing area of the thermal camera tracking system. A preliminary qualitative performance indicator is given in Fig. 6 (right), where two people are well tracked in our kitchen scenario.

6 Conclusions and Future Work

We have presented a people tracking system that is embedded into an ambient assisted living apartment. It could be shown that circular percepts coming from segmented thermal camera images are sufficient to *feed* Monte-Carlo particle filters for estimating the position of the persons to be tracked. A comparative experiment contrasted our approach with an high-precision optical marker tracking system, and revealed a mean tracking error of $\approx 12\,\text{cm}$.

To develop this promising approach towards a real solution requires redesign of the thermal camera to have wide angle to allow for low mounting positions, for instance. This is future work and also discussed below. The presented method already handles occlusions due to fixed infrastructure such as beams; using wide angle cameras, this could also be pillars or high appliances in the observed area. It is certainly not reasonable to manually specify the positions of such objects in the camera image as has been done in our experimental setup. It rather requires a calibration phase of the camera to detect these, but is conceivable.

That said, the results show that a sufficiently accurate tracking of multiple persons can be achieved using low-cost thermal cameras. For instance, in museums or shops, it allows to easily track peoples walking paths and length of stays at points of interests. By combining the people tracking with information about actuators in the environment allows to develop pro-active environment assistance, such as to automatically adjust the illumination. Finally, it can be used to realize safety mechanisms, such as to detect unconscious persons, which is a side-effect of the background subtraction: the blob tracking a person losing consciousness vanishes over time due to the background subtraction. Hence, vanishing blobs, which are in the middle of a camera image, can be used as indicators. To avoid false-positives requires to adjust the parameter used in background subtraction such that common durations of immobility do not lead to blob disappearance, and to combine tracking information with information over the environment, to exclude areas where people typically rest, such as sofas or beds.

Since the overall tracking system proposed in this paper involves various methods, future work is manifold. Starting with the preprocessing of thermal

images, segmentation could be improved by integrating dynamic adjustment of the segmentation threshold. Applying a shape-based classifier for pixel-blobs, instead of abstracting to circular percepts, would enable us to better discriminate not only persons from other sources of heat, but also persons in different postures, e.g. standing vs. sitting. Because of the thermal camera's narrow field of view, a tracking system covering the whole apartment asks for integrating multiple cameras. This extension will require a new layer of abstraction that allows single particles from instantiated filters to *move* from one camera view to another. In this context, we want to keep in mind that the unusual high mounting position of the thermal camera system used, is due to its quite low field of view. For lower mounting positions, not only wide angle lenses are necessary, but also a perspective correction of raw images, which could be neglected in this work.

Acknowledgement. Special thanks go to Felix Wenk and Jan Janssen who supported us in setting up the A.R.T. DTrack2 tracking system for evaluation.

References

1. Advanced Realtime Tracking GmbH. ARTTRACK System (2015). http://www.ar-tracking.com/products/tracking-systems/arttrack-system/
2. Autexier, S., Hutter, D., Mandel, C., Stahl, C.: SHIP-tool live: orchestrating the activities in the bremen ambient assisted living lab. In: Augusto, J.C., Wichert, R., Collier, R., Keyson, D., Salah, A.A., Tan, A.-H. (eds.) AmI 2013. LNCS, vol. 8309, pp. 269–274. Springer, Heidelberg (2013)
3. Bazzani, L., Bloisi, D., Murino, V.: A Comparison of multi hypothesis kalman filter and particle filter for multi-target tracking. In: Performance Evaluation of Tracking and Surveillance workshop at CVPR, pp. 47–54, Miami, Florida (2009)
4. Eisa, S., Moreira, A.: Requirements and metrics for location and tracking for ambient assisted living. In: 2012 International Conference on Indoor Positioning and Indoor Navigation (IPIN), pp. 1–7, November 2012
5. FLIR Systems Inc. FLIR LEPTON Long Wave Infrared (LWIR) Datasheet (2015). http://cvs.flir.com/lepton-data-brief?_ga=1.148414963.572252733.1449483173
6. Fox, D., Burgard, W., Dellaert, F., Thrun, S.: Monte carlo localization: efficient position estimation for mobile robots. In: Proceedings of the National Conference on Artificial Intelligence (AAAI), pp. 343–349 (1999)
7. Future-Shape GmbH. SensFloor large-area sensor system (2015). http://www.future-shape.com/en/technologies/23/sensfloor-large-area-sensor-system
8. Grisetti, G., Stachniss, C., Burgard, W.: Improved techniques for grid mapping with rao-blackwellized particle filters. IEEE Trans. Rob. **23**(1), 34–46 (2007)
9. Hevesi, P., Wille, S., Pirkl, G., Wehn, N., Lukowicz, P.: Monitoring household activities and user location with a cheap, unobtrusive thermal sensor array. In: Proceedings of the 2014 ACM International Joint Conference on Pervasive and Ubiquitous Computing, UbiComp 2014, pp. 141–145. ACM, New York (2014)
10. Krieg-Brückner, B., Röfer, T., Shi, H., Gersdorf, B.: Mobility assistance in the bremen ambient assisted living lab. GeroPsych J. Gerontopsychology Geriatr. Psychiatry **23**(2), 121–130 (2010)

11. Kumar, S., Marks, T.K., Jones, M.: Improving person tracking using an inexpensive thermal infrared sensor. In: 2014 IEEE Conference on Computer Vision and Pattern Recognition Workshops (CVPRW), pp. 217–224, June 2014
12. Röfer, T., Laue, T.: On B-human's code releases in the standard platform league – software architecture and impact. In: Behnke, S., Veloso, M., Visser, A., Xiong, R. (eds.) RoboCup 2013. LNCS, vol. 8371, pp. 648–655. Springer, Heidelberg (2014)
13. Voigt, M.: Monte-Carlo Lokalisierung im Innenraum mittels Bluetooth Low Energy basiertem Fingerprinting. Master's thesis, University of Bremen, May 2015
14. Wolfram MathWorld - the web's most extensive mathematics resource. Circle-Circle Intersection 2015. http://mathworld.wolfram.com/Circle-CircleIntersection.html

http://www.springer.com/978-3-319-39600-2

Inclusive Smart Cities and Digital Health
14th International Conference on Smart Homes and Health Telematics, ICOST 2016, Wuhan, China, May 25-27, 2016. Proceedings
Chang, C.K.; Chiari, L.; Cao, Y.; Jin, H.; Mokhtari, M.; Aloulou, H. (Eds.)
2016, XVII, 517 p. 199 illus., Softcover
ISBN: 978-3-319-39600-2